Surface Science 602 (2008) 2348–2357

Contents lists available at ScienceDirect

Surface Science

journal homepage: www.elsevier.com/locate/susc

# Structural studies of sub monolayer Sn/Cu(001) structures

J. Lallo [a], L.V. Goncharova [a], B.J. Hinch [a,*], S. Rangan [b], R.A. Bartynski [b], D.R. Strongin [c]

[a] Department of Chemistry and Chemical Biology, Laboratory of Surface Modification, Rutgers University, NJ 08854, United States
[b] Department of Physics and Astronomy, Laboratory of Surface Modification, Rutgers University, NJ 08854, United States
[c] Department of Chemistry, Temple University, Philadelphia, PA 19122, United States

ARTICLE INFO

*Article history:*
Received 28 November 2007
Accepted for publication 22 April 2008
Available online 7 May 2008

*Keywords:*
Atom-solid scattering and diffraction-elastic
Scanning tunneling microscopy
Surface relaxation and reconstruction
Surface stress
Surface structure, morphology, roughness, and topography
Copper
Tin
Adatoms

ABSTRACT

Helium atom scattering (HAS) and scanning tunneling microscopy (STM) have been used to investigate five ordered phases formed by Sn-evaporation and deposition on room temperature Cu(001) surfaces. Complementary Auger (AES) and electron diffraction (LEED) studies have also been performed. Glide plane symmetry has been noted in a p(2 × 6) phase. The c(4 × 8), p(3√2 × √2), and c(4 × 4) phases exhibit measurable lateral relaxations. The c(4 × 8) and c(4 × 4) phases have Sn in distorted nearest-neighbor adsorption sites. New structural models are proposed for four Sn/Cu phases. Each of these models is discussed in light of the lateral stress relief mechanisms that are operative. STM topographic details are used to argue in favor of the prevalence of 2-D alloy-like structures in most phases. We speculate also on the necessity of subsurface vacancies in formation of the *p2mg*, p(2 × 6) ordered phase.



## 1. Introduction

The ordering of metallic adsorbates on copper surfaces has been subject to much study [1–3]. In part because of the well known 3-D bronze alloy, the structure and properties of *tin* films on copper surfaces have been extensively investigated, both in submonolayer [4–8] and multilayer [9,10] coverage regimes. The large lattice mismatch between tin and copper contributes to a complex yet well defined series of ordered phases formed with room temperature Sn exposure of Cu(001). ($a_{Sn}$ is ~10% greater then $a_{Cu}$.) LEED studies [4,11] of the Sn/Cu(001) system have identified five room temperature Sn super-structures; i.e. the "p(2 × 2)", p(2 × 6), c(4 × 8), p(3√2 × √2) and c(4 × 4) phases. These were observed between 0.24 ML and 0.7 ML coverages of Sn. No ordered structures have been reported with room temperature Sn levels in excess of 0.7 ML. In contrast to Sn on Cu(001), Sn on Cu(111) does not exhibit such a rich phase diagram [6].

Both helium atom scattering [12] (HAS) and scanning tunneling microscopy [13] (STM) have been used to study similar bi-metallic systems. This paper concentrates explicitly on the interpretation of these techniques' observations from the ordered Sn/Cu(001) phases. We report here a new symmetry requirement for the p(2 × 6) phase and the first real-space images of the c(4 × 8), p(3√2 × √2) and c(4 × 4) phases. This new information places additional constraints on the overlayer structure models and we suggest new models for some phases.

It is has been reported that 2-D alloying occurs for at least some of the sub monolayer coverage Sn/Cu(001) phases [14]. In simple substitutional surface alloy formation, lateral stress levels must grow as the Sn densities increase [15]. Consequently, all alloy superstructures will exhibit means for stress relief within these phases. In this paper we raise the possibility of another distinct means, to be added to the commonly accepted catalog of possible lateral stress relief mechanisms, that may be active in the Sn/Cu(001) system. Finally, based on the argument that increasing in-plane vacancy densities must increase monotonically with Sn density, we are able to arrive at one sequence of models that is consistent with all observations, and thus represents our best assignments for the structure of each room temperature Sn/Cu(001) phase. We suggest that the approach used here may be applicable also to other alloying systems which exhibit rich phase diagrams.

## 2. Experimental

Two ultra-high vacuum chambers were used to obtain the results presented in this work. LEED, AES, and high-resolution HAS studies were conducted in the first system, and STM, LEED and

* Corresponding author. Tel.: +1 732 445 0663.
*E-mail address:* jhinch@rutchem.rutgers.edu (B.J. Hinch).

0039-6028/$ - see front matter © 2008 Elsevier B.V. All rights reserved.
doi:10.1016/j.susc.2008.04.028

AES data were acquired in a second system. Both UHV chambers had base pressures of below $2 \times 10^{-10}$ Torr.

In both systems, Cu(001) crystals were cleaned by 30 minute cycles of 600 eV $Ar^+$ sputtering followed by 850K annealing. A higher sputtering voltage (1500 V) was often needed to remove the residual surface tin atoms. After sputter cleaning, no surface tin, oxygen or carbon contaminants were observed, as measured by Auger spectroscopy.

In the first system, which has been described in detail elsewhere, [16] tin deposition was first monitored in helium atom specular, $\Theta_i = \Theta_f = 49.5^o$, reflectivity measurements, over a range of substrate temperatures. A maximum in helium atom reflectivity curves was ascribed to the completion of the $p(3\sqrt{2} \times \sqrt{2})$ phase at a Sn coverage of 0.5 ML, and all coverages were referenced to this coverage. (All of our data is consistent with this assertion.) The Sn deposition was also monitored with a quartz crystal microbalance, and Auger measurements were taken with a PHI double pass cylindrical mirror analyzer. Auger spectra were recorded after each deposition and ratios, between the Sn(MNN) and Cu(LMM) peak features at 430 eV and 920 eV, respectively, were used for relative coverage determination. The Auger feature ratio was used also for direct comparison with measurements taken in the second UHV system. The Auger ratio was found to be proportional to the Sn coverage, for all but the $c(4 \times 4)$ phase. This highest coverage phase exhibited a slightly enhanced Sn to Cu Auger ratio.

The second system consists of a UHV Omicron VT Scanning Probe Microscope connected with UHV sample transfer to a sample preparation/analysis chamber. The latter chamber includes LEED, Auger, sputtering ion gun, and metal evaporation sources. The same Sn-evaporation source from the HAS measurements was used in this chamber, and Sn deposition was monitored by a quartz crystal monitor (QCM). The Sn coverages were calibrated by using Auger peak intensity ratios as in the other system. LEED was used to confirm surface structure formation. All STM measurements were performed at room temperature and, in contrast to step-edge images which were seen for a wide range of tunneling conditions, Sn structures were reproducibly observed only in a narrow range of low voltage and high current conditions. All STM images shown in this paper were taken at ~+5 mV tip bias and ~7 nA tunnel current and in a constant current tunneling mode.

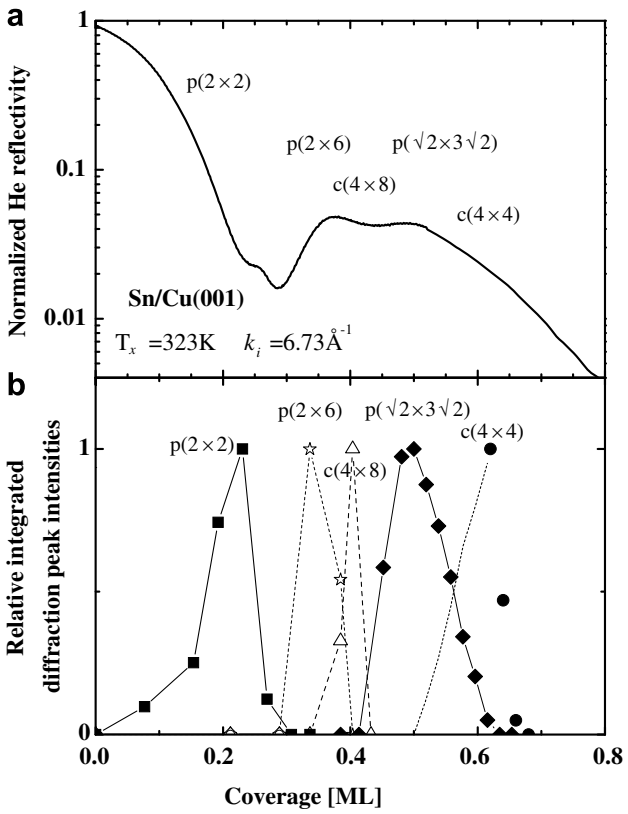


**Fig. 1.** He diffraction intensities scattered from Cu(001) at 300 K, and at varying Sn coverages. (a) He specular reflectivities normalized to that of the clean surface. The scattering geometry was aligned along the $[1\bar{1}0]$ azimuth. Total uptake curve duration shown, 5 min. (b) Integrated diffraction peak intensities, using diffraction peaks of identified phases taken along both [100] and $[1\bar{1}0]$ azimuths using $E_i = 23.65$ meV, $k_i = 6.73$ Å$^{-1}$. Discrete peaks used are listed in the text. Integrated intensities are approximated by $\Sigma_{peaks} I \bullet FWHM^2$. With the exception of the $c(4 \times 4)$ phase (see text), the "integrated intensities" are then normalized to their maximum value (for each phase.) In both (a) and (b) cumulative coverages are scaled such that the $p(\sqrt{2} \times 3\sqrt{2})$ phase is maximized at 0.5 ML of Sn.

## 3. Results and discussion

He atom specular reflectivity was monitored during Sn uptake. For samples at room temperature, the complex structure of these curves, such as shown in Fig. 1(a), is indicative of a sequence of ordering phenomena. Local intensity maxima are indicators of completion, or near completion, of ordered phases. Sequential He diffraction scans show many of these phases can coexist, but the following order of phases with increasing Sn coverage is adhered to: what we refer to as "$p(2 \times 2)$", $p(2 \times 6)$, $c(4 \times 8)$, $p(3\sqrt{2} \times \sqrt{2})$ and $c(4 \times 4)$ phases, respectively. At least one report of studies on each of these phases is found in the literature.

The uptake curves in specular reflectivity vary slightly with uptake rate. For example, we have observed that the relative specular intensity of the $p(3\sqrt{2} \times \sqrt{2})$ phase is almost tripled if the Sn deposition rate is reduced to ~0.016 ML/min. Kinetic limitations in surface restructuring are implied, particularly of this 0.5 ML phase. The shape of the uptake curve also has a dependence on the scattering azimuth. This is a non kinematic effect, implying the significance of He multiple scattering in scattered intensities from at least some of the ordered phases.

Although we report evidence for kinetic effects in phase formation, we have found no direct evidence for simultaneous coexistence of three or more ordered phases on the surface. The coexistence of only two ordered phases at any time is fully consistent with diffraction intensity observations. Normalized integrated diffraction peak intensities are shown in Fig. 1(b), and were determined using the following diffraction peaks; the split diffraction maxima at ~(1/2,1/2) for the "$p(2 \times 2)$" phase: (1/3,0) and (2/3,0) for $p(2 \times 6)$: (1/4,0) and (3/4,0) for $c(4 \times 8)$: (2/6,2/6) and (5/6,5/6) only for $p(3\sqrt{2} \times \sqrt{2})$. For the $c(4 \times 4)$ phase the (1/2,1/2) peak intensity is used only *after* complete loss of the $p(3\sqrt{2} \times \sqrt{2})$ phase.

Unlike the other preceding lower coverage phases, it is not certain if the $c(4 \times 4)$ phase can be formed in the absence of a coexisting phase. Below 0.625 ML some $p(3\sqrt{2} \times \sqrt{2})$ phase is always present. At higher coverages the integrated peak intensities decrease immediately, suggesting increased disorder and formation of a presumed multilayer phase (without measurable diffraction peak intensities). At a Sn coverage of ~0.7 ML even the specular feature is almost absent. Thus, we cannot be certain that the $c(4 \times 4)$ phase can fill the entire surface. Therefore, in Fig. 1(b), the points of the $c(4 \times 4)$ phase use a different means of normalization. Generally, the normalized integrated diffraction peak intensities are meant to be suggestive of fractional surface areas coverage, of each phase. The sum of fractional areas, at any coverage, should not exceed one. Consequently, for the $c(4 \times 4)$ phase, the dashed line rising from 0.5 ML to 0.61 ML is simply a curve given by $1-x$, where $x$ = the values for the $p(3\sqrt{2} \times \sqrt{2})$ phase,

and is provided only to guide the eye (i.e. possible significant surface fractions of disordered regions are ignored.) Given this supposition, relative specular diffraction intensities of each of the phases are tabulated in Table 1.

### 3.1. Sn/Cu(0 0 1) surface structure observations and plausible models

In the following section we discuss our observations made, and introduce viable models, for each known ordered phase. Some models suggested have been presented elsewhere yet we show that, even with much enhanced information provided here, definitive structural models cannot be given. A broader overview of these structures is presented section, III.C.

#### 3.1.1. p(2×2)

Our STM images of the low coverage incommensurate p(2 × 2) phase are fully consistent with that of earlier work by Cafolla et al. [14] and we do not present our data here. Using STM and X-ray standing wave data they concluded that p(2 × 2) patches of dimension 8 × 8 $a_{Cu}{}^2$, are separated by Cu like domain wall regions several $a_{Cu}$ wide. Here $a_{Cu}$ denotes the nearest-neighbor distance, 2.55 Å. The regularly spaced light domain walls act as a means of stress relief between p(2 × 2) patches, which can be presumed to be under compressive stress within a overlayer. They have also suggested that the domain walls can become narrower and enable the Sn densities to approach 0.25 ML. Additional stress relief results from a rumpling in the p(2 × 2) regions where the Sn atom centers are raised with respect to the Cu atoms within the 2-dimensional like alloy phase. We suggest also that such a rumpling contributes towards the inability of STM, including our own measurements, to resolve Cu atoms within surface alloy phases.

#### 3.1.2. p(2 × 6)

The p(2 × 6) phase is readily observed in electron and helium atom diffraction but has proven more difficult to image in the STM. Akin to the "p(2 × 2)" phase, which exhibits domain wall regions of the superstructure that show considerable dynamic disorder, we presume all areas covered by the p(2 × 6) phase show comparable mobility. As a consequence, diffraction patterns have proven to be more informative about the structure of the p(2 × 6) phase than STM images. Fig. 2(a) shows a two-dimensional helium diffraction pattern of a surface where both the p(2 × 6) and c(4 × 8) phases coexist. Importantly, we find an absence of intensity at ((2n+1)/6, 0) diffraction positions, although diffraction peaks are present with momentum transfers out of the plane containing [1$\bar{1}$0] and the surface normal directions; namely ((2n+1)/6, ½) and ((2n+1)/6, 1) features are present. Note a (3/6, 0) intensity is observed in Fig. 2(a), arising both from the second domain of the p(2 × 6) phase and from the coexisting c(4 × 8) phase. The c(4 × 8) phase gives the most intensity in Fig. 2(b) since helium diffraction from the p(2 × 6) alone shows only a very weak (1/2, 0) feature, as is apparent from Fig. 2(d). The absence of intensity at the other ((2n + 1)/6, 0) positions, checked for incident helium energies between 21 meV and 34 meV, implies a *p2mg* symmetry for the p(2 × 6) phase. This observation has not reported before, presumably as the p(2 × 6) phase is so often in coexistence with the c(4 × 8) phase and the location of the missing diffraction features are often obstructed from view in many LEED systems. Consistent with *p2mg* symmetry, we have not found visible (5/6,0) or (1/6,0) intensities in either our SPALEED investigations (90–130 eV) nor in any published LEED data [9,11].

With the realization of a glide plane within the p(2 × 6) phase, all previously reported suggested models for this phase must be discounted. Instead we suggest three new possible Sn unit cell models with *p2mg* symmetry, consistent with the observed diffraction peak positions. The first model, depicted in Fig. 3(a), is an overlayer composed of all Sn atoms sitting in bridge adsorption sites. In this image, and all following images of this paper, the light orange colored circles represent Cu atoms, and the darkest red circles represent Sn. This overlayer structure, with a copper coverage in the topmost layer, $\Theta^1_{Cu} = 0$, seems implausible as alloy-like structures will be presumed for lower- and, higher-Sn coverage phases. A second model, shown in Fig. 3(b), utilizes the same bridge adsorption sites for the Sn, but the top layer is now alloyed with a finite density of Cu atoms, ($\Theta^1_{Cu} = 0.333$), shown with darker orange circles. The density of these alloying Cu atoms must be limited, as the relatively large displacement of Sn from fourfold hollow sites imply the total number density of atoms within the topmost layer must be much less than a pure Cu top layer ($\Theta^1_{Cu+Sn} < 1$).

In contrast, a third model is proposed in Fig. 3(c), with only small displacements of Sn atoms from fourfold sites. This model can therefore support more alloying Cu atoms ($\Theta^1_{Cu} = 0.666$), allowing a ($\Theta^1_{Cu+Sn} = 1$). This 2-D alloy layer would be unfavorable without any means for stress relief. We propose that the stress is relieved through the introduction of vacancies within the second layer. We shall see that those vacancies also give rise to the displacement pattern with the required glide plane symmetry.

We believe that the third model is unusual in character and requires additional discussion. As emphasized in Fig. 3c, it is based on a c(2 × 6) structure, with alternating stripes of p(2 × 2) and c(2 × 2) character. The pattern of small Sn displacements from idealized fourfold hollow sites in an otherwise complete alloy layer, indicated with arrows in Fig. 3c, then reduces the overall unit cell symmetry from *c2mm* to the required *p2mg*. We have concluded that such Sn displacements of the required symmetry can only be induced by 1/6th ML of "interaction centers" located anywhere above or below certain hollow sites on the surface. Such "interaction centers" can be adsorbate species above these surface sites or substrate vacancies below them. We propose the latter scenario, and suggest a 3 × 2 array of second layer vacancies (Cu absences), as depicted by the small dots of Fig. 3c. These vacancies then allow a relaxation of Cu, and Sn above. In this albeit speculative model, the smaller (Cu) atoms of the alloy layer are better able to drop into the lower layer. This relaxation induces an increased separation of

**Table 1**
Normalized specular He reflectivities, of the room temperature deposited Sn on Cu(0 0 1) phases, relative to that of clean Cu(0 0 1)

| Surface structure | Sn coverages of proposed superstructures (ML) | Coverage range of experimental observation (ML) | Sn coverages at maximized diffraction intensities (ML) | Normalized $I_{(00)}$ plotted in Fig. 1(a). Uptake rate ~0.16 ML/min | Normalized $I_{(00)}$ from angular scans taken between Sn exposures (averaged rate ~0.016 ML/min) for collection of Fig. 1(b) data |
|---|---|---|---|---|---|
| "p(2 × 2)" | 0.25 | 0.08–0.27 | 0.23 | 0.025 | 0.03 |
| p(2 × 6) | 0.333 | 0.34–0.38 | 0.34 | 0.038 | 0.09 |
| c(4 × 8) | 0.375 | 0.38–0.41 | 0.40 | 0.046 | 0.07 |
| p(3$\sqrt{2}$ × $\sqrt{2}$) | 0.5 | 0.45–0.63 | 0.5 | 0.043 | 0.126 |
| c(4 × 4) | 0.625 | 0.55–0.66 | 0.615 | 0.02 | 0.03 |

Data is listed for the He incident energy, $E_i$ = 23.65 MeV, and room temperature phases.

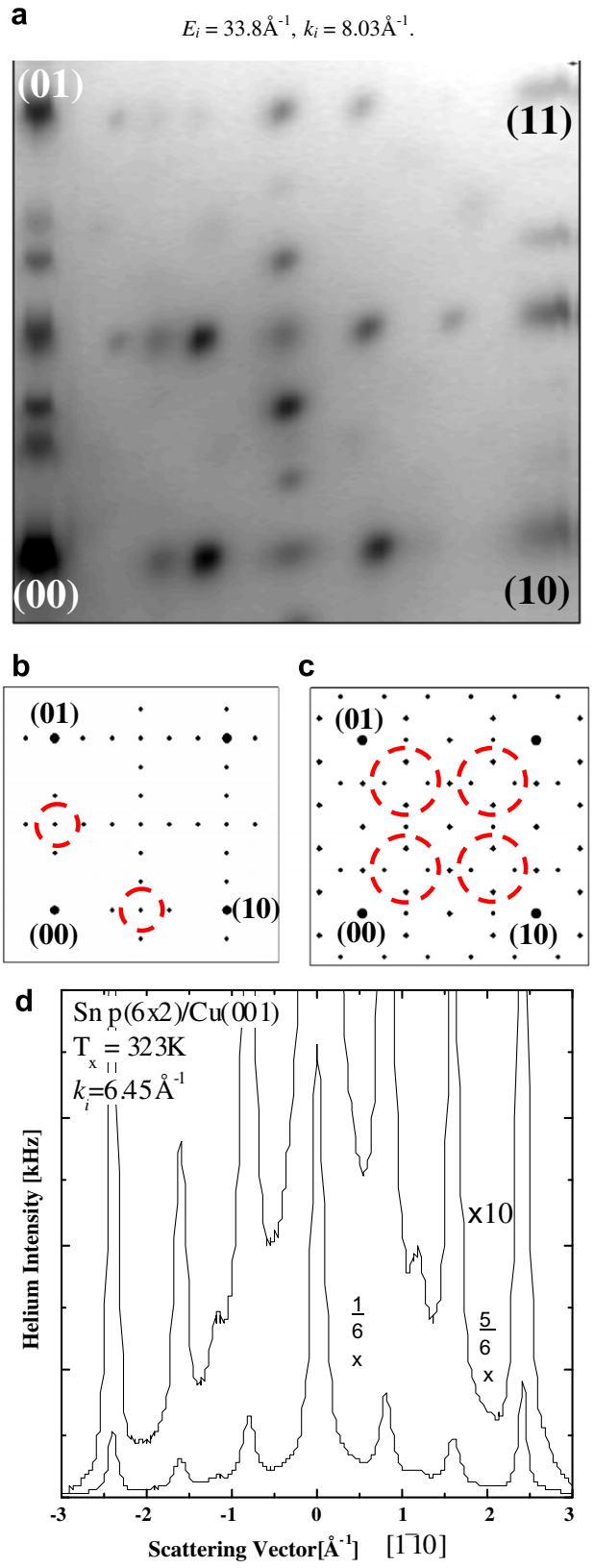


**Fig. 2.** (a) Gray scale image of a helium diffraction pattern measured at 0.38 ML Sn coverage, when the p(2 × 6) and c(4 × 8) phases coexist; (b) and (c) are schematic views of the p(2 × 6) and c(4 × 8) diffractions patterns, respectively. (Two domains of each phase are exhibited.) Highlighted (encircled) points are comparatively weak but are observable in these figures, (a) or (d). (d) A He angular distribution scan, along the [1 1 0] azimuth, for a pure p(2 × 6) Sn/Cu(0 0 1) surface structure at 0.34 ML Sn. (Quarter order spot intensities were not observed from this surface, as the c(4 × 8) phase is not initiated.) Note the absences of ±1/6 and ±5/6 diffraction peak intensities.

adjacent Sn atoms, along {1 0 0} directions, as shown in Fig. 3c. As the projections of these displacements along a direction perpendicular to the glide plane direction are only expected to be "small", certain diffraction intensity features should be comparatively small. Namely, as observed the (1/2, 0) diffraction intensities are anticipated to be much weaker than the (0, 1/3) and (0, 2/3) peaks, that is fully consistent with the observations, for example, as shown in Fig. 2d.

The low helium atom diffraction peak intensities, compared to the associated specular reflection intensities, are supportive of the more complete alloy layer models with low surface corrugations. It is mentioned that we have been unable to generate any other models for the p(2 × 6) phase, with high surface plane densities and the correct Sn density, while maintaining the correct unit cell dimensions. As the unit cell is of the (2 × n) type, models that contain glide planes running perpendicular to the 2× direction often reduce to a c(2 × n) superstructure. p(2 × 6) models that have been suggested by other authors invariably, erroneously, have *p2mm* symmetries. It is difficult to ascertain which of the two proposed Fig. 3 alloy p(2 × 6) structures is most likely correct. A simple kinetic analysis of LEED intensities could not be used to distinguish between the two models. LDA calculations of these and similar structures may give the best indication of which models are most appropriate in this system. Unfortunately we have not been able to record reliable STM images of this phase, yet it does still seem plausible that low temperature STM may still be able to distinguish models of Fig. 3a or Fig. 3b from that of Fig. 3c.

### *3.1.3. c(4×8)*

We report here the first real-space data recorded from a c(4 × 8) phase superstructure for this surface. This phase has recently been identified by only one other group using LEED [11], and they have reported on the thermal stability of this phase. The STM image of Fig. 4a illustrates an example of the ordered c(4 × 8) phase, in coexistence with more disordered regions with ~0.5 ML local coverage. Here twelve local maxima are clearly seen in the c(4 × 8) unit cell, consistent with the anticipated number density of Sn atoms, at a coverage of 0.375 ML. In all our STM images, we propose only Sn atoms are observed; Cu atoms of the top surface plane (if there are any) are too low to contribute to the imaged topograph. We note, however, that chemical contrast between substrate atoms and adsorbate elements in a surface has been observed in a number of other alloying systems (PtSn, [13] PdCu, [17] InCu [18], AgCu [10]).

The Sn atoms are not placed in identical sites. A group 4 of the 12 are seen to be comparatively high (raised by ~0.05 Å) in the topographs, and are displaced laterally, along [1 0 0] directions, from fourfold hollow sites. The majority Sn atoms sit much more closely to hollow sites. The approximate lateral position of the minority group's core is deduced from line scans such as those shown in Fig. 4b. This approach is subject to errors, for any peak position that is not in two perpendicular surface mirror planes. (Electronic and tip effects can change apparent positions, but not usually by as much as suggested here.) The minority group members appear to shift by $\delta \sim 0.64$ Å towards a bridge adsorption site. The closest Sn–Sn distances are reduced to ~3.2 Å. The relative raising of the minority Sn group members is brought about as the location of these atoms approaches a bridge site. (A compensating electron withdrawal height effect is also to be anticipated, which would reduce any anticipated geometric height increase.)

Fig. 5a is a hard sphere model that illustrates the observed Sn positions in this superstructure. The ordering may be viewed as one derived from a c(2 × 2) network of Sn atoms, but with 4 Sn atoms removed per centered unit cell, as indicated by the diamonds in Fig. 5a. This removal then allows the relaxation of 0.125 ML of Sn atoms, as seen by their strong displacements with

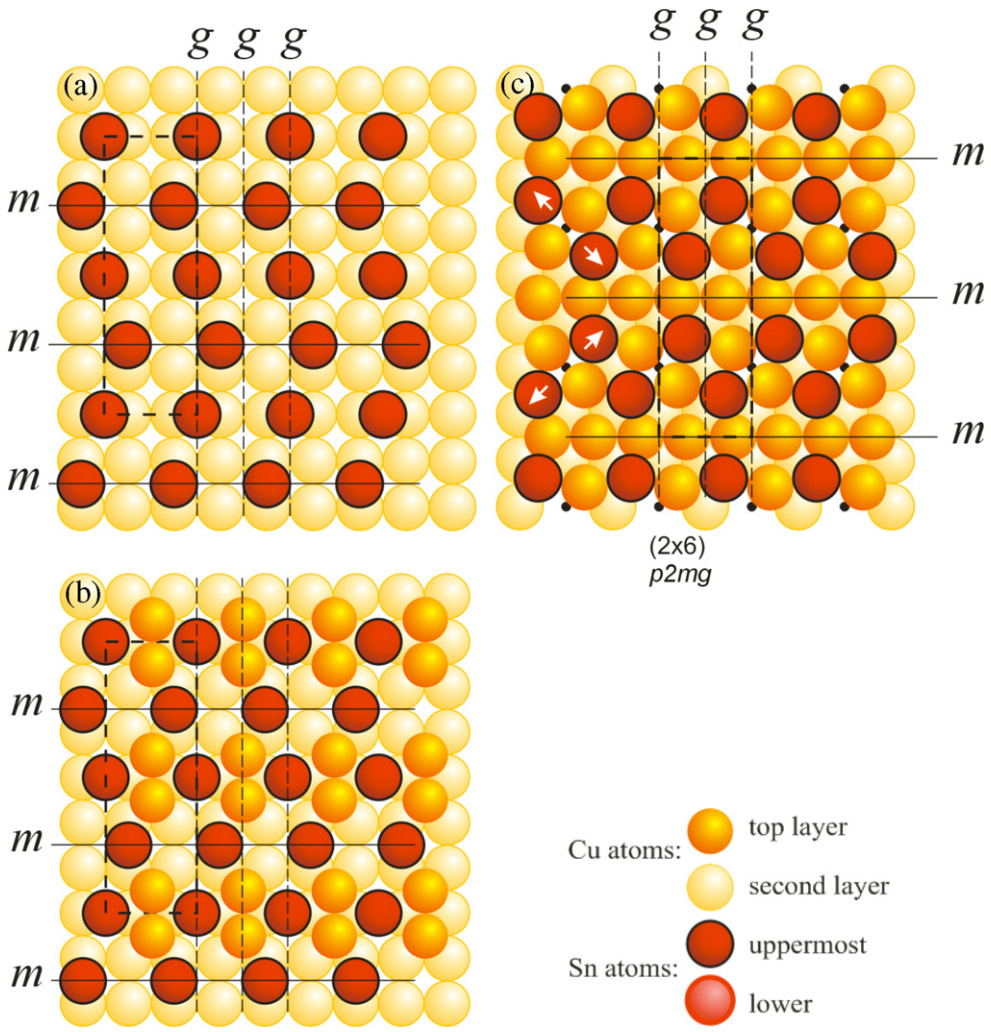


**Fig. 3.** Top view of model *p2mg* Sn p(2 × 6) structures. The unit cell is delineated by the dashed boxes. (a) A 0.33 ML Sn overlayer structure. (b) as (a) with added Cu atoms within the topmost layer. (c) Complete topmost layer with Cu vacancies in the sublayer (dots.) Arrows indicated Sn displacement directions. The key illustrates atomic species, and their relative heights. This key is applicable for Figs. 3, 5 and 7–9 also. "Lower Sn atoms" appear first in Fig. 5. Mirror planes ($m$) are shown with solid lines, glide planes ($g$) with dashed lines.

respect to the original c(2 × 2) network, i.e. the sites of the remaining Sn atoms in the majority group.

Since we assume the room temperature STM images are dominated by Sn positions alone, the surface Cu density cannot be determined directly. Yet the marked lateral displacement of the minority Sn atoms is a clear indication that a minimum of 0.125 ML of vacancies exists within the topmost layer. The two proposed models of this phase, shown in Fig. 5a and b, differ only in the number density of top plane copper atoms. Strictly speaking, the STM is unable to distinguish between the overlayer and alloy models of Fig. 5, although the deepest minima within the STM images are located at a position between "raised" Sn atoms, i.e. at the diamond positions shown in Fig. 5a.

We can also infer possible properties of the c(4 × 8) phase structure from our HAS data. The diffraction pattern from the c(4 × 8) phase, shown in Fig. 2, appears strongly (2 × 4)-like. Other diffraction features are comparatively weak. The He atoms are reflected from a surface corrugation function that, while it may not have the same Fourier amplitudes, is expected to have qualitative similarities to that shown in the STM image. A Fourier transform of the imaged STM topograph, however does not appear "strongly (2 × 4)-like" but has more c(2 × 2) and c(4 × 8) character. This discrepancy may be explained by noting that large fractions of the surface did not display this static image. In fact only very few c(4 × 8) patches were sufficiently stable to be imaged. We also note that these patches are constrained by areas of higher-Sn density. We suggest that the helium atoms are, in fact, scattering predominantly from possibly dynamic surface structures, though still with overall c(4 × 8) symmetry. One potential source for this instability may be the comparable ease for correlated motion [19] of "Sn-pairs" as illustrated by the arrows of Fig. 5a. The same correlated motion would be comparatively facile also in the alloy structure of Fig. 5b. All other atoms in the unit cell remain fixed and exhibit long range (2 × 4) ordering only. The 1/8th order diffraction intensities rely solely on the relative ordering of the Sn-pairs. Therefore, just as is seen in Fig. 2a, the 1/8th order features could be comparatively weak if the Sn-pair motion is thermally activated at room temperature. Such dynamic motion may also be the fundamental reason why the ordered c(4 × 8) was not observed over the majority of the surface with STM.

Martínez-Blanco et al. have shown that the c(4 × 8) phase is not stable above ~360 K [11]. Their LEED patterns show a high temperature phase they describe as p(2 × 2). However, only the (1/2,1/2) diffraction peaks remain sharp; the (1/2,0) peaks are considerably streaked (an effect that is apparent also at 300 K.) Unfortunately, it is not clear over what temperature range any eighth order intensities persist on their surface, indicating stable c(4 × 8) superstructures [11]. The c(4 × 8) structure may be most pronounced only

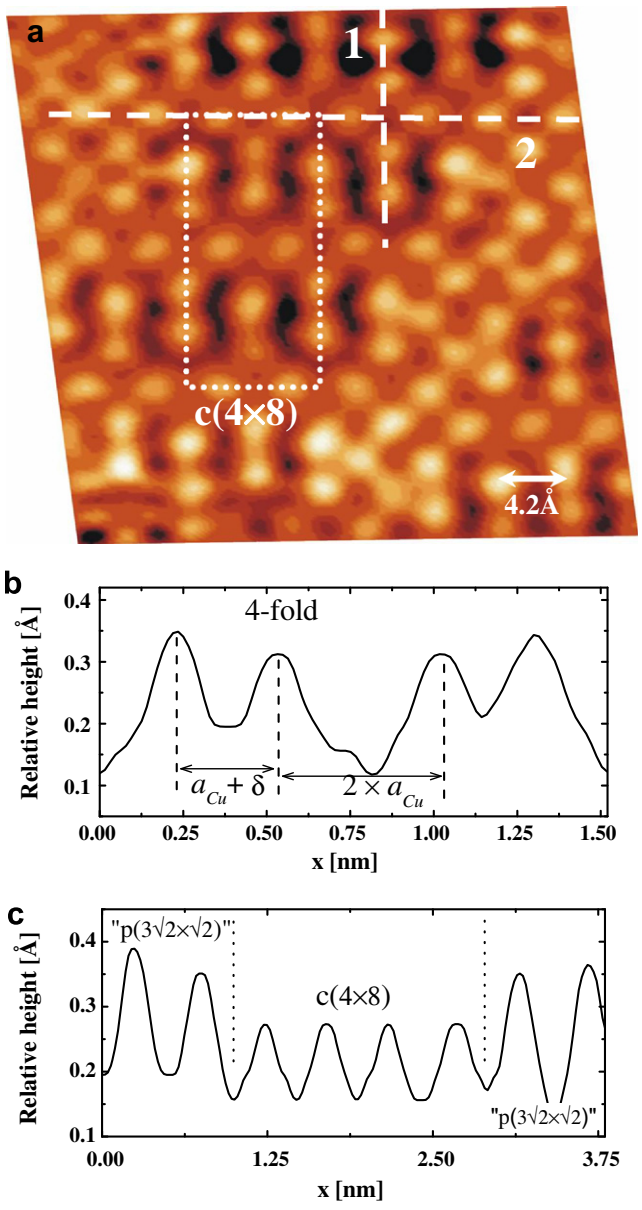


**Fig. 4.** STM topography image of 0.4 ML Sn/Cu(001). (a) Scan size is 40 × 40 Å. The unit cell is shown by a dotted line. Dash lines (1) and (2) indicate the cross-sections that are displayed in (b) and (c). The dimension, $a_{Cu} + \delta = 3.2+/-0.2$ Å $a_{Cu} = 2.55$ Å

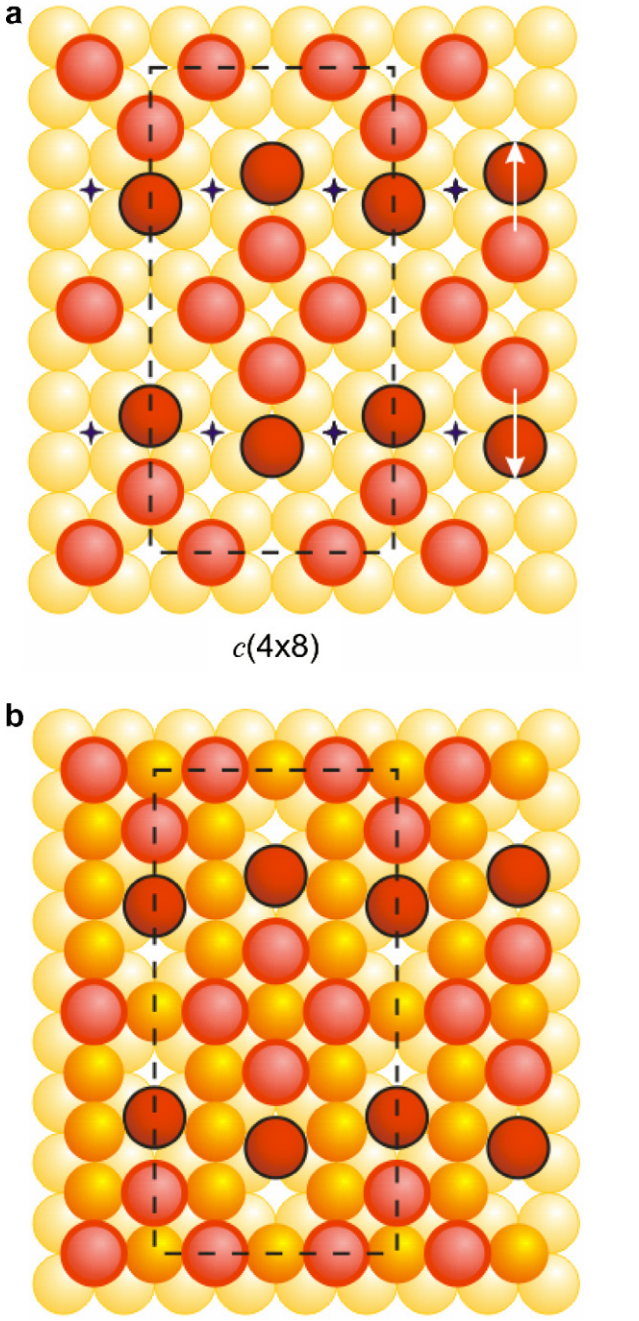


**Fig. 5.** Top view of Sn/Cu(001) c(4 × 8) models. Unit cells are shown by the dashed lines. Atom coloration: see the key of Fig. 3. (a) An overlayer structure. Diamonds and arrows are discussed in the text. (b) A Sn Cu alloy structure.

at lower temperatures, or under conditions where all Sn positions are locked in. Defects and/or adjacent patches of other-Sn-density phases may be the only way of stabilizing large areas of this phase for direct observation in STM.

*3.1.4. p(3√2 × √2)*

The next ordered phase, at 0.5 ML Sn coverage, is the most stable and is the one that has been seen after a wide range of thermal processing. An STM image, of this p(3√2 × √2) phase, is shown in the top and left sections of Fig. 6a. Once again only Sn atoms are imaged. A line scan through the p(3√2 × √2) region is shown in Fig. 6b. Again, from a simple interpretation of peak maxima positions we deduce that Sn atoms are displaced laterally, from four-fold hollow sites along [1$\bar{1}$0] directions, by as much as 0.35 ± 0.1 Å. The lower and adjacent Sn atoms are separated by only 2.95 Å.

This p(3√2 × √2) phase can also be viewed as one derived from a c(2 × 2) pattern of Sn atoms, but with additional displacements of 2/3 of the Sn atoms in [100] directions inducing the larger scale, p(3√2 × √2) periodicity. The pattern of imaged Sn atoms is illustrated in the Sn overlayer model of Fig. 7a. Dynamic LEED simulations [8] have indicated a commonly accepted alloy model, illustrated in Fig. 7b. In the latter model lateral displacements are induced due to a regular array of missing Cu atom rows in an otherwise c(2 × 2) alloy phase. However, from STM and HAS alone there remains some ambiguity with respect to the surface Cu density. Indeed our STM images are fully consistent with the model suggested in Ref. [8], however the possible alternative structure, as shown in Fig. 7a, is equally viable. We believe this overlayer structure, with subsurface missing Cu atom rows, was not explicitly tested in the LEED simulations. The unusual subsurface missing

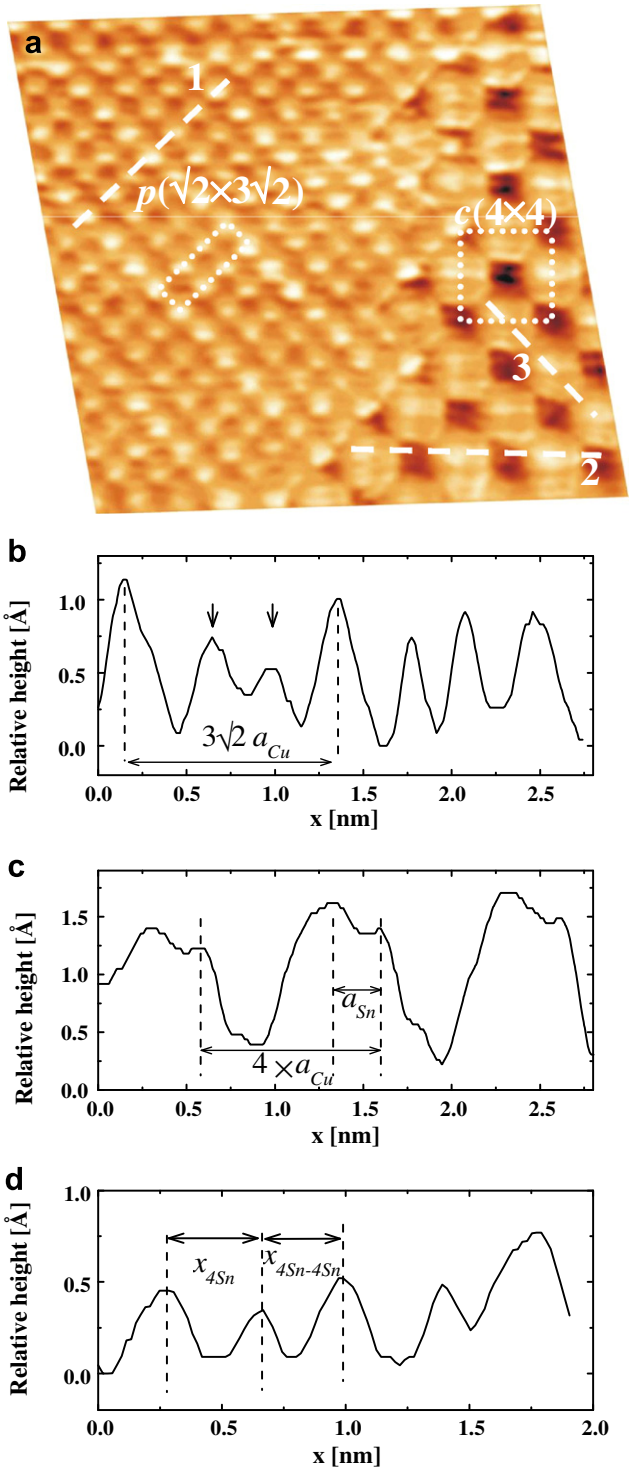


**Fig. 6.** (a) STM topograph of ~0.55 ML Sn/Cu(001). The scan size is 40 × 40 Å. Two unit cells are highlighted with dotted lines. The dashed line (1) indicates the position of the cross-section, in the p(3√2 × √2) phase, which is displayed in (b). In (b) the distance between the two maxima, designated by the arrows, is less than $\sqrt{2}\ a_{Cu}$. The dashed lines (2) and (3) indicate the cross-sections in the c(4 × 4) phase, along [1 $\bar{1}$ 0] and [100] azimuth directions, shown in (c) and (d). $a_{Cu}$ designates the Cu–Cu nearest-neighbor distance, 2.553 Å. $x_{4Sn}$ (3.9 Å) and $x_{4Sn-4Sn}$ (3.3 Å), respectively designate adjacent Sn–Sn [100] distances within and between the "4 Sn" clusters. $a_{Sn}$ designates the Sn–Sn [1 $\bar{1}$ 0] nearest-neighbor distance, ~2.75 ± 0.1 Å. The latter value was deduced from analysis of many line scans akin to that shown in (c).

Cu feature of Fig. 7b model is required to introduce the 3√2 periodicity lateral displacements observed in the top layer Sn atomic positions.

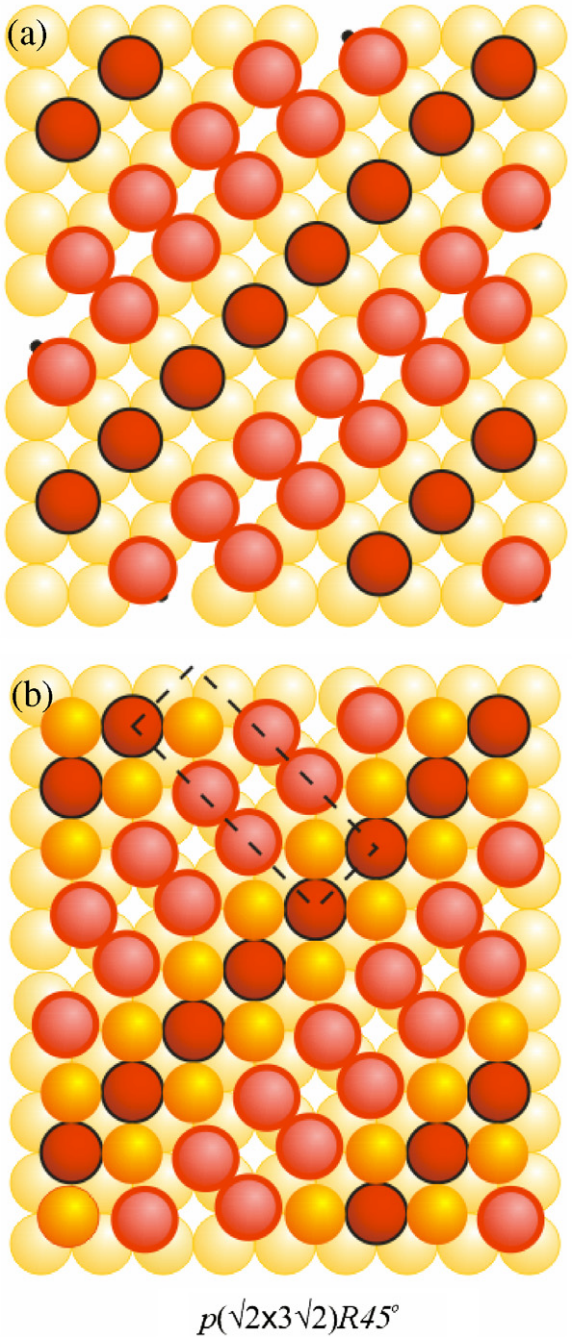


**Fig. 7.** Model p(3√2 × √2) phase structures. The unit cell is shown by dashed lines. (a) A Sn overlayer structure. (b) A Sn/Cu alloy structure. Both structures exhibit lateral displacements of some Sn atoms from fourfold hollow sites.

### 3.1.5. c(4 × 4)

The c(4 × 4), also described as a p(2√2 × 2√2)R45°, phase at 0.625 ML shows a qualitatively different STM image, as seen in the bottom right corner of Fig. 6a. The number density of high-Sn features also is not equal to the anticipated Sn density. A small fraction of the Sn atoms, $\Theta_{Sn}$ = 0.125 ML, do not appear within the STM image. The placement of this Sn in a lower layer, as indicated in Fig. 8 with pale red (pink) circles, can explain this observation. In this case, lateral displacements of upper Sn atoms from nearest-neighbor sites are again deduced from line scans, such as those shown in Fig. 6c and d. Displacements from hollow sites are observed along the [100] directions, with a magnitude of order

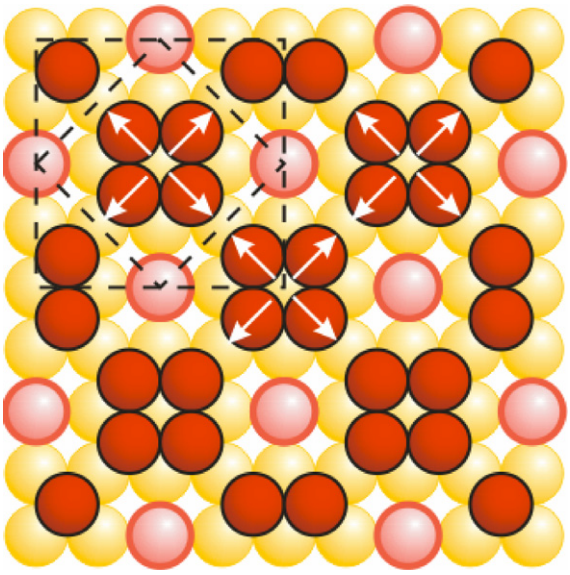

**Fig. 8.** Sn c(4 × 4) overlayer model. Centered and primitive unit cells are shown by the dash lines. Note two inequivalent Sn atom positions are present. Arrows indicate directions of observed lateral displacements, of overlayer Sn atoms, from fourfold hollow sites.

0.18 ± 0.07 Å. Nearest-neighbor $[1\bar{1}0]$ Sn–Sn distances now approach ~2.75 Å, in very close agreement with bulk Sn–Sn distances (~2.8 Å.) In HAS, this phase exhibits intense diffraction peaks at wide scattering angles. The corrugation function is presumed to be the highest of all observed phases. This view is supported by the fact that the highest observed STM corrugations, ~1.6 Å, are seen for this phase. This phase therefore has to be described as one that shows a combination of pure-overlayer and second layer alloying characters.

### 3.2. Surface stress relief mechanisms

In most of the phases investigated here, we have been able to suggest more than one viable structure. STM has shown to be useful in determining the Sn atom positions but its inability, at RT, to image Cu atoms still leaves some structural ambiguity. We discuss now stress relief mechanisms that may be operative in the RT Sn on Cu phases. In doing so we move towards a set of "preferred models" for each of the observed phases.

The tendency for alloy formation is apparent at low Sn coverages; Sn is seen in substitutional sites in the surface plane. In the absence of any operative stress relief mechanisms, as the (larger atomic radius) Sn density increases, surface stress levels would increase. At any Sn coverage, we presume that Cu and Sn do not remain coplanar, and that stress levels are mitigated via buckling of the outermost alloy layer, with Sn displaced further toward the vacuum compared to Cu cores. The final degree of buckling should follow directly the residual lateral stress in a surface plane. Direct evidence for film buckling has been seen for the "p(2 × 2)" phase [14]. Buckling is also seen in Cu(1 1 1), where Sn atoms are displaced from their nearest-neighbor substrate atoms perpendicular to the surface by 0.4 Å [6]. Simulations have also suggested buckling is present in the "p(2 × 2)" phase of Cu(0 0 1) [6]. As the local Sn density approaches 0.25 ML, lateral expansion of the topmost alloy layer starts to occur. This lateral expansion is not maintained over long distances. Patches of p(2 × 2) self organize with stress relieving lines of Sn-free copper. This model was introduced and discussed earlier [14]. Such long range ordering and method of stress relief is not seen in any other Sn/Cu phases.

An alternative stress relief mechanism, exhibited at higher-Sn exposures, appears to be partial if not complete ejection of Cu from a surface alloy. We might refer to an alloy phase if Cu expulsion is incomplete and to a Sn overlayer phase if Cu expulsion is complete.

Once top layer vacancies are formed, the Sn containing layer can undergo lateral relaxations, as is suggested for the alloy models of p(3√2 × √2) (Fig. 7b) and c(4 × 8) (Fig. 5b) structures. Note, lateral relaxations are plausible also in structures with any non-symmetric local atomic densities, as per the c(4 × 8)-overlayer and c(4 × 4) models, or in structures with lower layer vacancy formation, as per the suggested p(2 × 6)-alloy (Fig. 3c) or p(3√2 × √2)-overlayer (Fig. 7a) phases.

In our suggested models of Sn/Cu(0 0 1) phases, we have argued that small lateral relaxations are not necessarily indicative of in-plane vacancies. Formation of vacancies in a second plane is a less commonly accepted means for lateral stress relief, but we have invoked this mechanism in two models: once in an overlayer p(3√2 × √2) phase structure, and also in an alloy structure. A relaxation of top layer atoms towards second layer vacancies is the primary means for formation of the "Sn displaced" p(2 × 6) model, (Fig. 3c). Also, in favor of subsurface vacancy formation, second plane substitution is a requirement of the suggested c(4 × 4) structure at 0.625 ML. Such vacancy formation likely a necessary stage to 2nd layer alloying.

### 3.3. Sn/Cu(0 0 1) surface structures: a consistent overview

Salient features of some of our proposed Sn/Cu(0 0 1) models are summarized in Table 2 below. In the arguments below we shall

**Table 2**
Coverages within proposed models for known ordered room temperature Sn/Cu(0 0 1) phases

| Phase | "p(2 × 2)" | p(2 × 6) | | c(4 × 8) | | p(3√2 × √2) | | p(2√2 × 2√2) |
|---|---|---|---|---|---|---|---|---|
| Symmetry | **Incommensurate** | *p2mg* | | *c2mm* | | *p2mm* R45° | | *p4mm* R45° |
| Comment | | Sn-bridge 3b | **Sn displaced 3c** | over-layer 5a | **Alloy 5b** | over-layer 7a | **Alloy 7b** | aka c(4 × 4) |
| Illustration figure | | | | | | | | **8** |
| Local Sn coverage | <0.25 | 0.333 | | 0.375 | | 0.5 | | 0.625 |
| $\Theta^1_{Sn}$ | <0.25 | 0.333 | | 0.375 | | 0.5 | | 0.5 |
| $\Theta^1_{Cn}$ | >0.75 | 0.333 | 0.666 | 0 | 0.5 | 0 | 0.333 | 0 |
| $\Theta^1_{vac}$ | 0 | 0.333 | 0 | 0.625 | 0.125 | 0.5 | 0.166 | 0.5 |
| $\Theta^2_{Sn}$ | 0 | 0 | | 0 | | 0 | | 0.125 |
| $\Theta^2_{Cu}$ | 1 | 1 | 0.833 | 1 | | 0.666 | 1 | 0.875 |
| $\Theta^2_{vac}$ | 0 | 0 | 0.166 | 0 | | 0.333 | 0 | 0 |

$\Theta^n_X$ denotes the coverage of the X species in the *n*th layer. 2 models, discussed in the text, are given for each of the p(2 × 6), c(4 × 8) and p(3√2 × √2) phases. "vac" refers to vacancies in either first or second topmost layers. Phases highlighted with bold type are utilized later for Fig. 9.

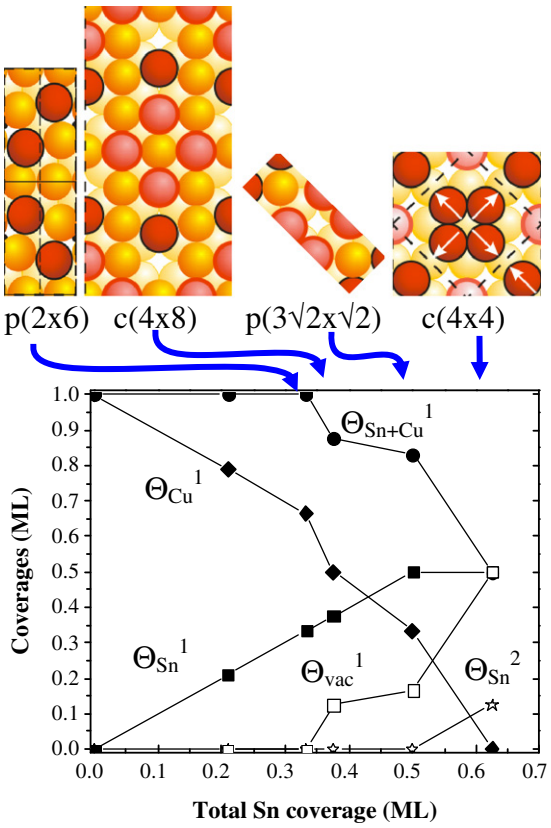


**Fig. 9.** Coverages within the preferred models for successive room temperature Sn/Cu(001) phases. $\Theta_X^n$ denotes the coverage of the X species in the *n*th layer.

concentrate on the top layer vacancy density, $\Theta_{vac}^1$, listed for each of the models.

In helping to assess the feasibility of various models of the p(2 × 6), c(4 × 8) and p(3√2 × √2) phases, we use two criteria. The first criterion is that values of $\Theta_{Sn} + \Theta_{Cu} + \Theta_{vac}$ must equal one for any given phase; i.e., each layer is whole. The second criterion is that each *component coverage* should be a *monotonic function* of total Sn coverage.

Fig. 9 illustrates coverage vs. total Sn coverage plots, for a particular series of five models highlighted in Table 2. Virtually all other combinations of models do not show this continuous behavior for $\Theta_{Sn}^1$, $\Theta_{Cu}^1$, and $\Theta_{vac}^1$ vs. $\Theta_{Sn}^{TOT}$ curves. Namely, the overlayer c(4x8) phase is discounted to prevent the $\Theta_{vac}^1$ curve from rising to 0.625 before falling to 0.5. Therefore the Sn-bridge p(2 × 6) model is also excluded as this would show oscillatory behavior in the $\Theta_{Cu}^1$ and $\Theta_{vac}^1$ curves with increasing Sn coverage. The only remaining uncertainty lies in ascribing the 0.5 ML phase to that shown in Figs. 7a or b. For the curves of Fig. 9, we have chosen to use the latter alloy phase (7b). Reasoning for this assertion is given below.

For increasing Sn number densities, at total coverages under 0.375 ML, the increased strain in ordered phases is accommodated by rumpling within the alloy layer or, when required, by the introduction of sublayer vacancies. At $\Theta_{Sn}$ = 0.375 ML the in-plane vacancy level, $\Theta_{vac}^1$, begins to rise to relieve higher stress levels. In alloy phases, the total density within the top layer is expected to affect the rumpling within any superstructure. The introduction of in-plane vacancies can enable a partially compensating reduction of rumpling of the remaining top layer. We now use this assertion to argue for an alloy phase (7b) at $\Theta_{Sn}$ = 0.5 ML. Indeed, alloy structures will be implied in both the 0.375 and 0.5 ML phases.

Two coexisting phases are displayed in Fig. 4a. Within this image, along the horizontal marked [100] direction line (2), the Sn density does not vary in going from the c(4 × 8) to an (albeit poorly ordered) 0.5 ML phase; Sn atoms appear regularly placed, with a lateral spacing of 2 $a_{Cu}$. The line scan of Fig. 4c indicates that the corrugation differs in the two phases, (with one identical scanning tip.) The overall height of the c(4 × 8), as well as the corrugation amplitude appears lower than that in its 0.5 ML neighboring regions. This reduction in corrugation is consistent with a decreased rumpling in an alloy type c(4 × 8) phase compared to that in a 0.5 ML alloy phase. We advocate the lower corrugation is related to the vacancy array within this phase, lateral relaxations, and a pressure reduction within the 2-D alloy. In contrast, overlayer structures are not expected to show such marked corrugation amplitude or absolute maxima height variations when the (very) local Sn atom densities appear unchanged. We conclude therefore that both 0.375 and ordered 0.5 ML phases have finite $\Theta_{Cu}^1$ levels (greater than zero,) consistent with our choice and use of alloy structures in Fig. 9.

It is only in the last phase, c(4 × 4), that $\Theta_{vac}^1$ has risen so high (0.5 ML) such that $\Theta_{Sn}^{TOT} + \Theta_{vac}^1$ must now exceed unity. This is accommodated by the incorporation of Sn into the second layer of this phase, when $\Theta_{Sn}^2 = 0.125$ ML.

## 4. Conclusions

STM imaging of binary superstuctures proves to be very powerful in assessing model plausibility. However, we have not found the technique to be able to unambiguously distinguish overlayer from alloy structures. While we have not been able to discount the overlayer p(3√2 × √2) phase, on the basis of good LEED *I–V* fits [8] and the local coverage dependent corrugation amplitudes of Fig. 4c, we have argued in favor of the most commonly accepted alloyed p(3√2 × √2) phase. One would conclude that the alloy phases are the more probable for all 0.2 to 0.5 ML phases. To satisfy the newly realized *p2mg* symmetry of the p(2 × 6) phase we have needed to invoke a 2nd layer vacancy formation. (Reproducible STM images have not been seen for this phase.) While this model remains speculative, the concept of lower lying vacancy formation, as yet another means for stress relief in alloy phases, may be applicable to many binary (or more complicated) superstructure systems. In addition, we have shown the presence of large lateral displacements, in c(4 × 8), (3√2 × √2) and c(4 × 4) phases, suggestive of in-plane vacancies. In-plane vacancy formation represents the most effective way of releasing in-plane stress levels, (for a given Sn density within alloy structures.) Thus we have argued that in-plane vacancy levels increase for increasing Sn coverage phases, whilst the degree of rumpling (for example) may not show such predictable Sn coverage variations. This latter argument has enabled us to give a unique "best series" of Sn/Cu(001) structural models.

## Note added in proof

Since submission of this paper it has come to our attention that some of the phases described and discussed in this paper have been imaged with room temperature STM and reported in an excellent, recent, but earlier, publication [Y. Nara, K. Yaji, T. Iimori, K. Nakatsuji, F. Komori, Surface Science 601 (2007) 5170.] These authors have presented very similar images of the 0.5 ML phase. They show also very similar images of c(4 × 8) patches, at coverages including 0.35 and 0.4 ML, and have deduced that top layer vacancies are present in this phase. Importantly too they were able to image the p(2 × 6) phase at room temperature at 0.33 ML. Their STM image of this phase is fully consistent with the model we have

proposed for the glide plane containing phase, of Fig. 3(c). Our paper goes further in reasoning for the alloy phase structures, the Cu vacancy densities, and also in images of the higher 0.625 ML phase. The helium diffraction here also gives complementary information about phase coexistence, and possible instabilities in these phases.

## Acknowledgement

This work was supported by the National Science Foundation, CHE 0517017.

## References

[1] D.D. Chambliss, S. Chiang, Surf. Sci. 264 (1992) L187.
[2] G.L. Kellogg, R. Plass, Surf. Sci. 465 (2000) L777.
[3] H.L. Meyerheim, H. Zajonz, W. Moritz, I.K. Robinson, Surf. Sci. 381 (1997) L551.
[4] E. McLoughlin, A.A. Cafolla, E. AlShamaileh, C.J. Barnes, Surf. Sci. 482–485 (2001) 1431.
[5] F. Abel, C. Cohen, J.A. Davies, J. Moulin, D. Schmaus, Appl. Surf. Sci. 44 (1990) 17.
[6] S.H. Overbury, Y.-S. Ku, Phys. Rev. B 46 (1992) 7868.
[7] C. Argile, G.E. Rhead, Surf. Sci. 135 (1983) 18.
[8] K. Pussi, E. AlShamaileh, E. McLoughlin, A.A. Cafolla, M. Lindroos, Surf. Sci. 549 (2004) 24.
[9] C. Argile, G.E. Rhead, Thin Solid Films 87 (1982) 265.
[10] P.T. Sprunger, E. Lagsgaard, F. Besenbacher, Phys. Rev. B 54 (1996) 8163.
[11] J. Martínez-Blanco, V. Joco, P. Segovia, T. Balasubramanian, E.G. Michel, Appl. Surf. Sci. 252 (2006) 5331.
[12] D. Farias, K.-H. Rieder, Rep. Prog. Phys. 61 (1998) 1575.
[13] M. Batzill, D. Beck, B.E. Koel, Surf. Sci. 466 (2000) L821.
[14] A.A. Cafolla et al., Surf. Sci. 544 (2003) 121.
[15] L.C. Feldman, K.W. West, B.M. Kincaid, Phys. Rev. Lett. 49 (1982) 1416.
[16] L.V. Goncharova, J. Braun, A.V. Ermakov, G.G. Bishop, D.M. Smilgies, B.J. Hinch, J. Chem. Phys. 115 (2001) 7713.
[17] P.W. Murray, L. Stensgaard, E. Lagsgaard, F. Besenbacher, Surf. Sci. 365 (1996) 591.
[18] T. Nakagawa, S. Mitsushima, H. Okuyama, M. Nishijima, T. Aruga, Phys. Rev. B 66 (2002) 085402.
[19] R.v. Gastel, E. Somfai, W.v. Saarloos, J.W.M. Frenken, Nature 408 (2000) 665.